Inorg. Chem. **2008**, *47*, 7327−7337

^{17}O Solid-State NMR and First-Principles Calculations of Sodium Trimetaphosphate ($Na_3P_3O_9$), Tripolyphosphate ($Na_5P_3O_{10}$), and Pyrophosphate ($Na_4P_2O_7$)

Filipe Vasconcelos,[†] Sylvain Cristol,[†] Jean-Francois Paul,[†] Grégory Tricot,[†] Jean-Paul Amoureux,[†] Lionel Montagne,[†] Francesco Mauri, and Laurent Delevoye*[,†]

UCCS-Unité de Catalyse et Chimie du Solide, UMR CNRS, 8181, École Nationale Supérieure de Chimie de Lille, Université des Sciences et Technologies de Lille, BP 108, 59652 Villeneuve d'Ascq Cedex, France, and Institut de Minéralogie et Physique des Milieux Condensés, Université Pierre et Marie Curie, Campus Boucicaut, 140 rue de Lourmel, 75015 Paris

Received April 8, 2008

The assignment of high-field (18.8 T) ^{17}O MAS and 3QMAS spectra has been completed by use of first-principles calculations for three crystalline sodium phosphates, $Na_3P_3O_9$, $Na_5P_3O_{10}$, and $Na_4P_2O_7$. In $Na_3P_3O_9$, the calculated parameters, quadrupolar constant (C_Q), quadrupolar asymmetry (η_Q), and the isotropic chemical shift (δ_{cs}) correspond to those deduced experimentally, and the calculation is mandatory to achieve a complete assignment. For the sodium tripolyphosphate $Na_5P_3O_{10}$, the situation is more complex because of the free rotation of the end-chain phosphate groups. The assignment obtained with ab initio calculations can however be confirmed by the $^{17}O\{^{31}P\}$ MAS-J-HMQC spectrum. $Na_4P_2O_7$ ^{17}O MAS and 3QMAS spectra show a complex pattern in agreement with the computed NMR parameters, which indicate that all of the oxygens exhibit very similar values. These results are related to structural data to better understand the influence of the oxygen environment on the NMR parameters. The findings are used to interpret those results observed on a binary sodium phosphate glass.

1. Introduction

Nuclear magnetic resonance (NMR) together with X-ray diffraction (XRD) are among the most powerful techniques to study the structure of phosphate-based compounds. Phosphates occupy an important place in oxide material solid-state chemistry. Indeed, phosphates can be found as glasses, ceramics, organic/inorganic hybrids, catalysts, gels, and so forth. In the case of amorphous forms of phosphates, NMR has the great advantage to probe the local environment of the nuclei and does not require any long-range order. ^{31}P nucleus is commonly used to characterize the coordination and cationic surroundings as its chemical shift strongly depends on these parameters. Moreover, ^{31}P isotope has 100% natural abundance, is NMR sensitive ($^{\gamma}/_{2\pi}$ = 17.235 MHz/T), and is a spin $^1/_2$ nucleus, so that a complete averaging of the anisotropic broadenings resulting from powder samples can be obtained by using magic-angle spinning (MAS). All of these elements make the ^{31}P an attractive nucleus for the structural study of phosphate compounds with NMR.[1] The usual strategy includes the preliminary determination of NMR parameters (chemical shifts) for a series of similar crystalline phosphate compounds to further interpret the broad resonances generally observed in amorphous and disordered materials.

Oxygen has a predominant role in the structure of inorganic materials. Its NMR-active isotope, ^{17}O, is a quadrupolar nucleus (with a nuclear spin $I = {}^5/_2$). This means that the nuclear nonspherical charge distribution interacts with the electric field gradient (EFG) at the nucleus. The knowledge of the EFG can help elucidate the structural characteristics such as coordination numbers and the geometry of the neighboring nuclei. Then, in the case of a negligeable chemical shift anisotropy with respect to the MAS speed, the ^{17}O MAS NMR can be characterized by

* To whom correspondence should be addressed. E-mail: laurent.delevoye@ensc-lille.fr.
[†] Université des Sciences et Technologies de Lille.

(1) Tricot, G.; Montagne, L.; Delevoye, L.; Palavit, G. In *Recent Advances in Solid-State NMR of Inorganic Polymeric Phosphate Materials*; De Jaeger, R., Gleria, M., Eds.; Nova Science Publishers, Inc.: New York, USA, 2007; Chapter 13, pp 663−710.

10.1021/ic800637p CCC: $40.75
Published on Web 07/22/2008

three NMR parameters: the isotropic chemical shift (δ_{cs}), the quadrupolar constant (C_Q), and the quadrupolar asymmetry (η_Q).

However, ^{17}O NMR is much less popular than ^{31}P NMR in solid phosphates because of several drawbacks: i) its low natural abundance (0.038%), ii) its low sensitivity ($^{\gamma}/_{2\pi} = -5.7716$ MHz/T), and iii) the fact that it shows, even under MAS conditions, a second-order quadrupolar broadening. An isotopic ^{17}O enrichment,[2,3] combined with the use of a very high magnetic field,[4] can partly circumvent these drawbacks. Furthermore, modern 2D experiments, that is, the multiple-quantum MAS[5,6] (MQMAS) and the satellite-transition MAS[7] (STMAS), which are dedicated to quadrupolar nuclei with half-integer spin quantum number, were developed to eliminate completely the residual second-order quadrupolar broadening and to give high-resolution spectra. The MQMAS experiment has the advantage of being easy to implement[8] even if it suffers from a lack of sensitivity of the triple-quantum excitation and reconversion transfers. STMAS can yield substantial signal enhancements compared to MQMAS, but the presence of the first-order quadrupolar interaction in the satellite transitions imposes a high degree of accuracy for the magic-angle setting. In recent years, the efficiency of these sequences has been greatly improved in many ways such that it is now possible to explore the structure through the NMR study of low-γ nuclei like ^{95}Mo,[9] ^{39}K, ^{25}Mg,[10] and of course ^{17}O (for a good review of ^{17}O NMR developments see ref 11).

The assignment and interpretation of the ^{17}O MAS spectra, even with a good signal-to-noise ratio and the use of high-resolution sequences at a very high magnetic field, may still be ambiguous due to the lack of an extensive database of NMR parameters for this nucleus. If such a ^{17}O database exists for a series of organic compounds,[12,13] it is much more time demanding to develop such a database for inorganic materials, as it is specific to the nature of the cationic environment. Since the pioneering studies on ^{17}O solid-state NMR,[14,15] empirical assignments have been used to interpret the NMR response in terms of the local environment. However, these empirical correlations collected in the literature must be used with caution when they are considered out of their initial range of application. In amorphous systems, the distribution of NMR parameters is often related to a distribution in bond lengths and angles.[2] They are well characterized in silicate materials[16] but much less in phosphates.

First-principles calculations are often carried out as a complement to the experimental and empirical approaches. Until recently, the first-principles calculations of ^{17}O NMR parameters had been applied to cluster systems (i.e., isolated molecules or solid aggregates) in silicates,[17,18] aluminosilicates,[19] and phosphates.[20,21] These studies reveal that the ^{17}O quadrupolar parameters depend mainly on the first coordination sphere surrounding the oxygen. For the chemical shift parameters, the first coordination sphere is not sufficient especially in ionic solids where the long-range electrostatic potential has a large influence. In such systems, the correct description of the charge density requires an increasing number of atoms to be defined in the cluster, resulting in a large increase of the required computational resources. Different alternatives can be used to circumvent this problem. Di Fiori et al.[22] have proposed an embedding scheme to take into account the electrostatic potential in cluster calculations of NMR shielding tensors. Another approach is to use the 3D periodicity of the solid with periodic Density Functional Theory (DFT) calculations, as proposed by Mauri et al.[23] to estimate the solid response to the presence of a uniform magnetic field. Later, the Gauge Including Projector Augmented Waves (GIPAW) approach by Pickard and Mauri[24] added, to this initial development, the PAW method.[25] This development gave access to the all-electron magnetic response in a pseudopotential formalism. This method has been confronted to experimental ^{17}O NMR for different materials including zeolites,[26] sodium silicates,[27] crystalline aluminosilicates,[28] calcium aluminosilicate glasses,[29] and minerals.[30,31]

In the present article, we will show how periodical DFT

(2) Zeyer, M.; Montagne, L.; Kostoj, V.; Palavit, G.; Prochnow, D.; Jaeger, C. J. *Non-Cryst. Solids* **2002**, *311*, 223.
(3) Flambard, A.; Montagne, L.; Delevoye, L. *Chem. Commun.* **2006**, 3426.
(4) Gan, Z.; Gorkov, P.; Cross, T. A.; Samoson, A.; Massiot, D. *J. Am. Chem. Soc.* **2002**, *124*, 5634.
(5) Frydman, L.; Hardwood, J. *J. Am. Chem. Soc.* **1995**, *117*, 5367.
(6) Medek, A.; Harwood, J. S.; Frydman, L. *J. Am. Chem. Soc.* **1995**, *117*, 12779.
(7) Gan, Z. *J. Am. Chem. Soc.* **2000**, *122*, 3242.
(8) Amoureux, J.-P.; Fernandez, C.; Steuernagel, S. *J. Magn. Reson.* **1996**, *A123*, 116.
(9) d'Espinose de Lacaillerie, J.-B.; Barberon, F.; Romanenko, K. V.; Lapina, O. B.; Le Pollès, L.; Gautier, R.; Gan, Z. *J. Phys. Chem. B* **2005**, *109*, 14033.
(10) Dowell, N. G.; Ashbrook, S. E.; Wimperis, S. *J. Phys. Chem. B* **2004**, *108*, 13292.
(11) Ashbrook, S.; Smith, M. E. *Chem. Soc. Rev.* **2006**, *35*, 718.
(12) Wu, G. *Prog. Nucl. Magn. Spect.* **2008**, *52*, 118.
(13) Lemaître, V.; Smith, M. E.; Watts, A. *Solid State Nucl. Magn. Reson.* **2004**, 26–215.
(14) Schramm, S.; Oldfield, E. *J. Am. Chem. Soc.* **1984**, *106*, 2502.
(15) Timkem, H. C.; Turner, G. L.; Gilson, J. P.; Welsh, L. B.; Oldfield, E. *J. Am. Chem. Soc.* **1986**, *108*, 7231.
(16) Clark, T. M.; Grandinetti, P. J.; Florian, P.; Stebbins, J. F. *Phys. Rev. B* **2004**, *70*, 064202.
(17) Clark, T. M.; Grandinetti, P. J. *Solid State Nucl. Magn. Reson.* **2005**, *27*, 233.
(18) Xue, X.; Kanzaki, M. *Phys. Chem. Minerals* **1998**, *26*, 14.
(19) Kubicki, J.; Toplis, M. *Am. Mineral.* **2002**, *87*, 668.
(20) Alam, T. M.; Segall, J. M. *J. Mol. Struc.: Theochem* **2004**, *674*, 167.
(21) Cherry, B. R.; Alam, T. M.; Click, C.; Brow, R. K.; Gan, Z. *J. Phys. Chem. B* **2003**, *107*, 4894.
(22) Di Fiori, N.; Orendt, A. M.; Caputo, M. C.; Ferraro, M. B.; Facelli, J. C. *Magn. Reson. Chem.* **2004**, *42*, S41.
(23) Mauri, F.; Pfrommer, B. G.; Louie, S. G. *Phys. Rev. Lett.* **1996**, *77*, 5300.
(24) Pickard, C. J.; Mauri, F. *Phys. Rev. B* **2001**, *63*, 245101.
(25) Blöchl, P. E. *Phys. Rev. B* **1994**, *50*, 17953–17979.
(26) Profeta, M.; Mauri, F.; Pickard, C. J. *J. Am. Chem. Soc.* **2003**, *125*, 541–548.
(27) Charpentier, T.; Ispas, S.; Profeta, M.; Mauri, F.; Pickard, C. J. *J. Phys. Chem. B* **2004**, *108*, 4147–4161.
(28) Gervais, C.; Profeta, M.; Babonneau, F.; Pickard, C. J.; Mauri, F. *J. Phys. Chem. B* **2004**, *108*, 13249–13253.
(29) Benoit, M.; Profeta, M.; Mauri, F.; Pickard, C. J.; Tuckerman, M. E. *J. Phys. Chem. B* **2005**, *109*, 6052–6060.
(30) Ashbrook, S. E.; Le Pollès, L.; Pickard, C. J.; Berry, A. J.; Wimperis, S.; Farnan, I. *Phys. Chem. Chem. Phys.* **2007**, *9*, 1587.
(31) Ashbrook, S. E.; Berry, A. J.; Frost, D. J.; Gregorovic, A.; Pickard, C. J.; Readman, J. E.; Wimperis, S. *J. Am. Chem. Soc.* **2007**, *129*, 13213.

calculations can help in the assignment and interpretation of ^{17}O solid-state NMR spectra of crystalline sodium phosphate compounds. We will then discuss the influence of short- and long-distance ordering in phosphates on the quadrupolar parameters, C_Q and η_Q, and the isotropic chemical shift δ_{cs}. The results will finally be used for a better understanding of the long-range disorder in a sodium phosphate glass system.

2. Experimental Section

2.1. Samples preparation. In a first step, two sodium phosphate glasses ($50Na_2O$-$50P_2O_5$ and $62.5Na_2O$-$37.5P_2O_5$) were prepared by quenching a mixture of Graham's salt ($(NaPO_3)_n$, Prolabo) and sodium carbonate (Na_2CO_3, Prolabo), melted at 900 °C for 1 h. Then, the ^{17}O enrichment process was performed by heating the glasses at 700 °C for 8 h in the presence of ^{17}O-enriched water vapor in a closed tubular furnace.[3] A statistical exchange between the oxygen atoms of the material and the ^{17}O atoms of the enriched vapor is achieved through hydrolysis and condensation reactions, summarized by the following equations:

$$P-O-P+H_2^{17}O \leftrightarrow P-^{17}O-H+P-O-H \quad (1)$$

$$P-^{17}O-H+P-O-H \leftrightarrow P-^{17}O-P+H_2O \quad (2)$$

Finally, pure crystalline sodium trimeta- and tripolyphosphates, $Na_3P_3O_9$ and $Na_5P_3O_{10}$, were prepared through the devitrification of the ^{17}O enriched glasses at 550 °C for 8 h. Sodium pyrophosphate, $Na_4P_2O_7$, was prepared through a solid-state reaction between diammonium hydrogen phosphate and sodium carbonate at 800 °C. The sample was ^{17}O-enriched under ^{17}O water vapor at 700 °C for 15 h.

The crystallinity and purity of the three samples were checked through X-ray powder diffraction and ^{31}P MAS NMR, in which the absence of broad signals indicates a complete crystallization.

2.2. NMR details. All ^{17}O MAS NMR experiments were performed at 18.8 T on a Bruker Avance II spectrometer with a Bruker 3.2 mm (rotor diameter) tri-γ probehead operating at 108.47 and 323.90 MHz for ^{17}O and ^{31}P, respectively. The ^{17}O MAS spectra were obtained using a selective pulse of 11 μs at a radio frequency (RF) field strength of 7.5 kHz. The excitation pulse was preceded by a Double Frequency Sweep (DFS) pulse[32] to enhance the central transition polarization for half-integer quadrupolar nuclei. The signal enhancement was achieved using a 3 ms DFS pulse sweeping between 200 and 800 kHz at an RF field amplitude of 50 kHz. The 3QMAS spectra were collected at a MAS speed of 23 kHz, using the Z-filter sequence,[8] which consists of two hard pulses of 3.5 and 1.25 μs at an RF field of 100 kHz, for triple-quantum excitation and reconversion, respectively, followed by a soft pulse of 11 μs at an RF field of 7.5 kHz. The t_1 step was set to the MAS period. The $^{17}O\{^{31}P\}$ heteronuclear multiple quantum coherence (HMQC) spectrum was acquired using the pulse sequence introduced by Massiot et al.[33] The ^{17}O selective $\pi/2$ and π pulses were set to 11 and 22 μs, respectively and the ^{31}P π pulse to 10.5 μs. The total evolution time under $^{17}O-^{31}P$ J coupling was set to 6 ms. All other relevant experimental parameters are given in the figure captions. The ^{17}O and ^{31}P chemical shifts are given in ppm with respect to tap water and 85% of H_3PO_4 in solution, respectively.

3. Calculation Methods

Calculations were performed using the PARATEC code at DFT level of theory.[34,35] We used the PBE[36] functional for the generalized gradient approximation (GGA) of the exchange-correlation functional. The potentials due to the ions are represented by norm-conserving Troullier−Martins pseudopotentials.[37] The electronical configuration involved in the construction of the pseudopotentials for the different nuclei ^{23}Na, ^{31}P, and ^{17}O are respectively { $2p^2$ $2p^6$ $3d^0$ }, { $3s^2$ $2p^{1.8}$ $3d^{0.2}$ }, and { $2s^2$ $2p^3$ } with respective core radii (in atomic unit) {1.8 1.49 1.8}, {2.0 2.0 2.0}, and {1.45 1.45}.

The electronic structure gives access to the electric field gradient (EFG) tensor through the reconstruction of the all-electron wave function that is obtained with the projector augmented wave (PAW) approach.[25,26] The EFG tensor V is then diagonalized to obtain the principal components V_{xx}, V_{yy}, and V_{zz} where by convention $|V_{xx}| < |V_{yy}| < |V_{zz}|$. These components are related to the quadrupolar coupling constant C_Q and the asymmetry parameter η_Q by $C_Q = eQ|V_{zz}|/h$ and $\eta_Q = (V_{xx} - V_{yy})/V_{zz}$, respectively, where Q is the nuclear quadrupole moment and h is the Planck constant. In the present work, we used $Q = -25.58 \times 10^{-31}$ m^2, which is the value proposed by Pyykkö.[38]

The calculation of the absolute chemical shielding was performed using *GIPAW* algorithms developed by Pickard and Mauri.[24] Experimental isotropic chemical shifts δ_{cs} and absolute isotropic chemical shielding σ are related through the definition of an isotropic reference shielding σ_{ref} defined by $\delta_{cs} = \sigma_{ref} - \sigma$. In the NMR community, it is commonly accepted to use liquid reference compounds to compare different experiments. In a computing approach, it would not be conceivable to achieve accurate results using a liquid reference compound. In most cases, an arbitrary choice of a solid reference compound or an isolated resonance from the unassigned spectrum is preferred. In the present work, we set the absolute chemical shift value to an unambiguous isolated resonance, as presented subsequently. The convergence test in absolute chemical shielding on simple model (sodium orthophosphate) shows that the convergence in ^{17}O NMR parameters is achieved for an energy cutoff of 100 Ry. For the integration on reciprocal space, we used a dense k-point grid ($3\times2\times3$ for $Na_3P_3O_9$, $3\times4\times1$ for $Na_5P_3O_{10}$, and $2\times4\times2$ for $Na_4P_2O_7$).

The calculation of NMR parameters requires the accurate knowledge of the structure. However, the published crystallographic data for $Na_3P_3O_9$ and $Na_5P_3O_{10}$ were obtained with a poor precision using the Weissenberg film technique.[39,40] For all model systems, we here compared in a systematic

(32) Iuga, D.; Schafer, H.; Verhagen, R.; Kentgens, A. *J. Magn. Reson.* **2000**, *147*, 192.
(33) Massiot, D.; Fayon, F.; Alonso, B.; Trebosc, J.; Amoureux, J.-P. *J. Magn. Reson.* **2003**, *164*, 160.
(34) Pfrommer, B.; Raczkowski, D.; Canning, A.; Louie, S. G.; Mauri, F.; Cote, M.; Yoon, Y.; Pickard, C. J.; Heynes, P. PARATEC (PARAllel Total Energy Code).
(35) Kohn, W.; Sham, L. *Phys. Rev.* **1965**, *140*, 1133.
(36) Perdew, J. P.; Burke, K.; Ernzerhof, M. *Phys. Rev. Lett.* **1996**, *77*, 3865.
(37) Trouillier, N.; Martins, J. L. *Phys. Rev. B* **1991**, *43*, 1993.
(38) Pyykkö, P. *Mol. Phys.* **2001**, *99*, 1617.
(39) Ondik, H. *Acta Crystallogr.* **1967**, *18*, 226.
(40) Corbridge, D. *Acta Crystallogr.* **1967**, *13*, 263.

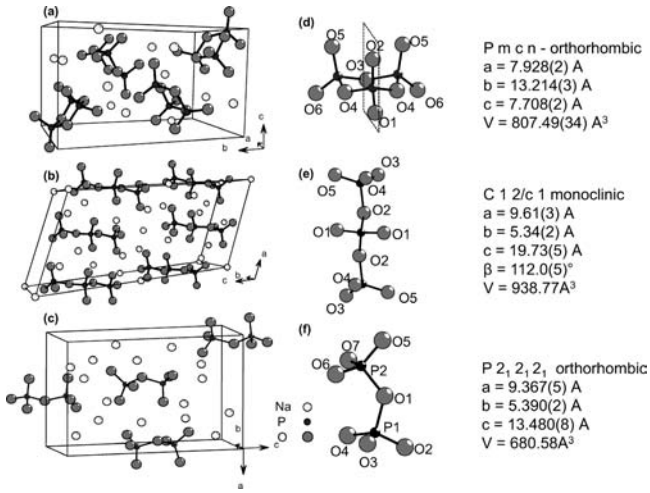

Figure 1. Unit cells of (a) $Na_3P_3O_9$, (b) $Na_5P_3O_{10}$, (c) $Na_4P_2O_7$. The basic anionic unit is shown in (d), (e), and (f) for $Na_3P_3O_9$, $Na_5P_3O_{10}$, and $Na_4P_2O_7$, respectively. Cell parameters and the notation employed for nonequivalent oxygen sites are those given in the original papers.[39,40,48] For $Na_3P_3O_9$, the mirror plane is indicated by a dashed line.

way the NMR parameters calculated directly from the original XRD structure with the ones obtained after DFT structure optimization. We used the VASP code[41–43] for the structure optimization, with GGA-PW91[44] functional and the PAW[45] scheme to describe the electrons-ions interaction (with $E_{cut} = 600$ eV and same k-points grid as for the NMR calculations). We took into account all the degrees of freedom (ionic internal coordinates, cell shape, and cell volume) for structure optimization, and we rescaled cell parameters to the experimental volume to avoid the DFT tendency to overestimate both the distances and the cell volume. This overestimation only affects the quadrupolar constant C_Q because of the direct dependence of this parameter upon the absolute V_{zz} value. On the other hand, the chemical shift and the asymmetry parameter η_Q are only weakly affected because they are relative values by definition.

4. Structural Data

The structure of sodium trimetaphosphate $Na_3P_3O_9$, was solved by Ondik in 1965[39] using single-crystal XRD (part a of Figure 1). It crystallizes in the orthorhombic *Pmcn* space group with four formula units per unit cell. The basic unit, $Na_3P_3O_9$, is composed of two crystallographically distinct sodium sites, two phosphorus sites, and six oxygen sites. It has been studied previously through ^{23}Na MAS NMR by Koller et al.[46] The ^{31}P MAS spectrum exhibits two resonances at −16.2 and −19.2 ppm, in a 1:2 ratio, in good agreement with crystallographic data. The basic anionic unit, as depicted in part d of Figure 1, is composed of a ring of three phosphate groups. Three oxygen sites, O1, O2, O3, are located on a symmetry plane represented by a dashed line in part d of Figure 1. These sites have a multiplicity of 1. The other sites, O4, O5, O6, which are located on either side of the symmetry plane, show a multiplicity of 2. Two types of oxygen sites can be distinguished: bridging oxygens (O3 and O4) that denote oxygen atoms connected to two phosphorus, and nonbridging oxygens (O1, O2, O5 and O6) that are connected to one phosphorus, only. Following the conventional notation, all phosphate entities in $Na_3P_3O_9$ are noted Q^2 because they are connected to two other phosphate groups.

The structure of the high-temperature form of sodium tripolyphosphate $Na_5P_3O_{10}$ (phase I), was determined by Corbridge in 1960 using single-crystal XRD.[40] The compound crystallizes in a monoclinic *C*2/*c* space group with four formula units per unit cell (part b of Figure 1). The ^{31}P MAS NMR[47] reveals the presence of two ^{31}P sites at 1.3 and −7.5 ppm with relative intensities 2:1 in agreement with the presence of Q^1 and Q^2 phosphate groups. The ^{23}Na MQMAS NMR[47] reveals the presence of three ^{23}Na sites, which is in agreement with the crystal structure. The anionic unit is formed of a chain of three phosphate groups (part e of Figure 1). Two of these phosphate groups are noted Q^1 as they are end-chain phosphates, and the third phosphate group is a central phosphate, Q^2, connected to two other phosphate units. Five crystallographically distinct oxygen sites can be distinguished. One site, denoted O2, is a bridging oxygen and the others are nonbridging oxygen sites, one of them being bonded to the Q^2 phosphorus (O1), the three others bonded to a Q^1 phosphorus (O3, O4, O5).

The structure of the sodium pyrophosphate (or tetrasodium diphosphate) $Na_4P_2O_7$ was determined by Leung et al.[48] in 1972 using single-crystal XRD. The structure is described in an orthorhombic $P2_12_12_1$ space group with four formula units per unit cell (part c of Figure 1). The ^{31}P MAS NMR spectrum and ^{23}Na MQMAS NMR spectra respectively reveals the presence of two and four crystallographically nonequivalent sites as expected from the structure. The two ^{31}P sites are separated by 0.5 ppm. The anionic unit is formed of two Q^1 phosphate groups (P1 and P2), connected through a bridging oxygen denoted O1. The other six oxygen sites are nonbridging oxygens (O2 to O7).

5. Results

5.1. Trimetaphosphate $Na_3P_3O_9$. Figure 2 brings together all ^{17}O NMR measurements of $Na_3P_3O_9$. The top spectrum in part a of Figure 2 shows the 1D ^{17}O MAS spectrum. The line shape is characteristic of half-integer quadrupolar nuclei MAS spectra broadened by second-order quadrupolar interaction. The sharp discontinuities reveal the high degree of crystallinity of the sample. To increase the resolution, a 2D 3QMAS spectrum (part b of Figure 2) was acquired. In the MAS dimension of part b of Figure 2, nonbridging oxygens are in the 50 to 85 ppm chemical shift range, whereas the large resonance on the left, which spans from 60 to 120 ppm,

(41) Kresse, G.; Hafner, J. *Phys. Rev. B* **1993**, *48*, 13115.
(42) Kresse, G.; Furthmuller, J. *Phys. Rev. B* **1996**, *54*, 11169.
(43) See http://cms.mpi.univie.ac.at/vasp/.
(44) Perdew, J. P.; Burke, K.; Wang, Y. *Phys. Rev. B* **1996**, *54*, 16533.
(45) Kresse, G.; Joubert, D. *Phys. Rev. B* **1999**, *59*, 1758.
(46) Koller, H.; Engelhardt, G.; Kentgens, A. P. M.; Sauer, J. *J. Phys. Chem.* **1994**, *98*, 1544.
(47) Fyfe, C.; zu Altenschildesche, H. M.; Skibsted, J. *Inorg. Chem.* **1999**, *38*, 84.
(48) Leung, K. Y.; Calvo, C. *Can. J. Chem.* **1972**, *50*, 2519–2526.

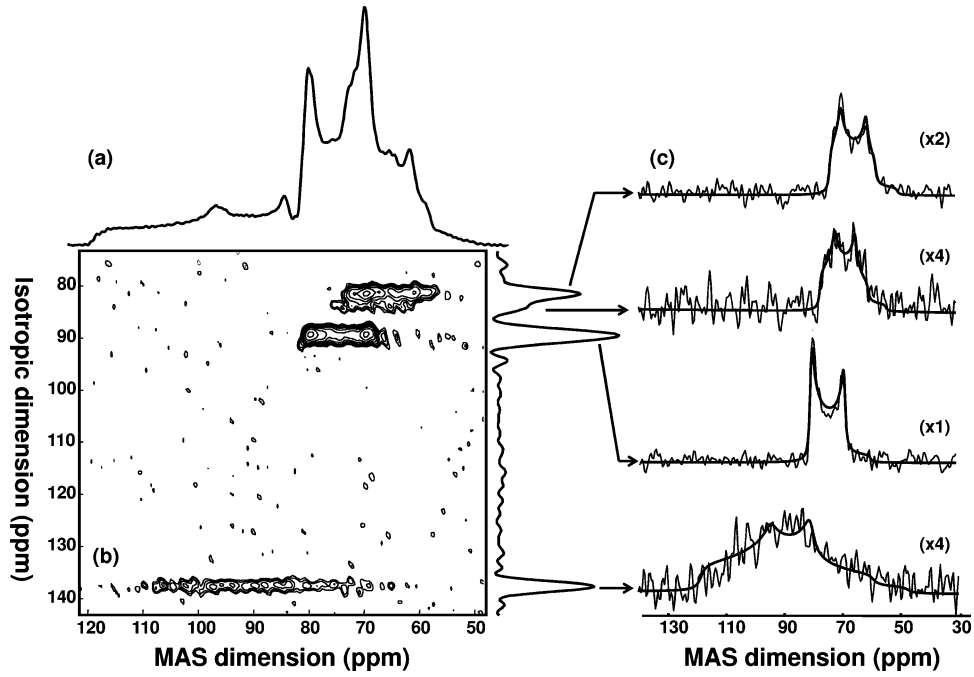

Figure 2. [17]O NMR of $Na_3P_3O_9$ (18.8 T). (a) The [17]O MAS spectrum was obtained after the accumulation of 832 scans with a recycling delay of 60 s. (b) A total of 96 scans was accumulated with a recycling delay of 20 s and 125 transients in the t_1 domain for an experimental time of ~66 h. (c) [17]O isotropic spectrum is shown together with the extracted individual slices and corresponding fit simulations.

Table 1. NMR Parameters Extracted by Fitting Each Individual Resonance of the MQMAS Spectrum of $Na_3P_3O_9$ and $Na_5P_3O_{10}$[a]

compound	C_Q (MHz)	η_Q	δ_{cs} (ppm)
$Na_3P_3O_9$	4.5	0.3	75.5
	4.3	0.4	77.5
	4.3	0.1	84.0
	~7.0	0.6	120.2
$Na_5P_3O_{10}$	4.5	0.2	79.5
	4.5	0.2	85.3
	~6.5	~0.6	~126

[a] The sites are organized from low to high chemical shifts. The accuracy of the measurement varies significantly depending on the intensity of the individual resonance. Nevertheless, the uncertainty does not exceed the following values: $C_Q \pm 50$ kHz; $\delta_{cs} \pm 0.5$ ppm; $\eta_Q \pm 0.05$).

typically corresponds to bridging oxygens. The isotropic projection (δ_{iso} scale) of the 3QMAS spectrum reveals the presence of two groups of nonbridging oxygens, around $\delta_{iso} = 82$ and 90 ppm, and a unique resonance at $\delta_{iso} = 138$ ppm corresponding to bridging oxygens. In this first approach, the empirical attribution was made based on the work by Zeyer et al.[2] who have shown that, in phosphate glass systems, bridging oxygens can be separated from nonbridging oxygens through their quadrupolar constant C_Q and their chemical shift δ_{cs}. The individual anisotropic cross section, together with their best-fit simulations, are shown on part c of Figure 2. Table 1 summarizes the NMR parameters resulting from the deconvolution of each resonance of the 3QMAS spectrum. One can notice that the shoulder on the isotropic resonance at $\delta_{iso} = 85$ ppm has been considered as an additional site, even though the low signal intensity renders difficult the determination of the NMR parameters (especially η_Q, which is directly related to the shape of the resonance). The present results finally reveal the presence of a total of four oxygen sites that are nonequivalent from a pure NMR point of view. There is a clear difference between the number of sites experimentally observed through [17]O NMR (4) and the ones expected from the XRD structure (6).

Table 2. Relative Intensities Extracted from the Fit of the 1D Spectra

compound	site	relative intensity (%)
$Na_3P_3O_9$	O6	22.5
	O1	11.6
	O2, O5	33.5
	O3	11.3
	O4	21.1
$Na_5P_3O_{10}$	O1	20.9
	O3, O4, O5	59.5
	O2	19.6

Table 3. DFT-GIPAW Calculated [17]O Quadrupolar Coupling Constant (C_Q), Quadrupolar Asymmetry (η_Q) and Isotropic Chemical Shift (δ_{cs}) Parameters Using DFT-Optimized Structure of $Na_3P_3O_9$ and $Na_5P_3O_{10}$[a]

compound	site	C_Q (MHz)	η_Q	δ_{cs} (ppm)
$Na_3P_3O_9$	O6	4.78	0.26	75.5
	O1	4.65	0.31	78.2
	O5	4.62	0.09	84.3
	O2	4.74	0.07	84.4
	O3	7.72	0.61	124.8
	O4	7.51	0.66	126.9
$Na_5P_3O_{10}$	O1	4.87	0.15	79.9
	O3	4.91	0.12	89.3
	O4	4.89	0.19	86.0
	O5	4.85	0.25	88.8
	O2	7.36	0.66	136.7
$Na_4P_2O_7$	O1	7.31	0.62	132.67
	O2	4.84	0.10	81.24
	O3	4.80	0.17	80.94
	O4	4.85	0.12	75.83
	O5	4.93	0.16	78.38
	O6	5.03	0.21	74.37
	O7	5.03	0.18	75.25

[a] The sites are organized from low to high chemical shifts.

[17]O NMR parameters resulting from our DFT-GIPAW calculation are given in Table 3. All calculated chemical shifts are shifted by a constant value to match the calculated value for O6 with the lowest experimental resonance

observed on the 3QMAS spectrum (δ_{cs} = 75.5 ppm). All values are consistent with those extracted from the 3QMAS spectrum (Table 1). The calculated and experimental quadrupolar asymmetry parameters η_Q are close, or at least within an acceptable accuracy if we consider the low signal intensity of sites O1 and O3/O4. The calculated quadrupolar coupling constants C_Q are also consistent with the empirical assignment of the bridging (~7 MHz) and nonbridging sites (~4.5 MHz), even if they are found slightly larger by 0.3−0.5 MHz than expected for such site environments. It must be noticed that such deviations (<0.2 MHz) were previously observed for silicates.[26,28,31] This result can be partly due to the fact that the DFT calculated quadrupolar constants, which are calculated at 0 K, are obtained without taking into account the thermal motions that occur during the NMR experiment.[49,50]

The calculated chemical shifts must be considered carefully. From the 3QMAS spectrum, the presence of an additional intermediate nonbridging site with δ_{cs} = 77.5 ppm is suggested. It is clearly confirmed by first-principles calculations as the site denoted O1. The DFT calculation further brings to light the similarity of sites O2 and O5 in terms of the NMR parameters. These two sites correspond to the single resonance observed at δ_{cs} = 84.0 ppm on the 3QMAS spectrum. The two bridging oxygen sites, O3 and O4, are found to be separated by ~2 ppm even though a single oxygen site is detected at first sight on the MQMAS spectrum. Furthermore, it appears that calculated bridging oxygen chemical shifts are overestimated by ~5−7 ppm with respect to the experimental values. This deviation for bridging oxygen is only due to the fact that here, a nonbridging oxygen site, O6, is chosen as chemical shift reference.

Finally, Figure 3 shows the fit of the experimental spectrum using the calculated values as a starting point. We observed that a scaling factor needs to be applied to the computed chemical shift to match the experimental ones. The correlation presented in the discussion section (Figure 9) leads to the value of 0.88. All calculated C_Q were reduced by 0.3 MHz for the reasons given above. The relative ratio of the different oxygen sites are those expected from the structure (Table 2). The resulting calculated and experimental MAS spectra exhibit identical most-intense discontinuities. The accuracy of the DFT calculation for site O1 also leads to a good overall picture of the small discontinuities. Furthermore, it was possible to separate O3 and O4 sites in the experimental spectrum at the expense of a long experimental acquisition of 12 h. This is exhibited in the inset of Figure 3, which shows a shoulder around 118 ppm with the correct relative intensity for O3 and O4 sites.

5.2. Tripolyphosphate $Na_5P_3O_{10}$. The ^{17}O 1D MAS spectrum shown in Figure 4 for $Na_5P_3O_{10}$ reveals the presence of a splitting of less than 1 ppm in the nonbridging oxygen region, proving the excellent crystallinity of our sample. This splitting, which leads to an observed spreading of the 2D 3QMAS lineshapes (Figure 5) in the region of

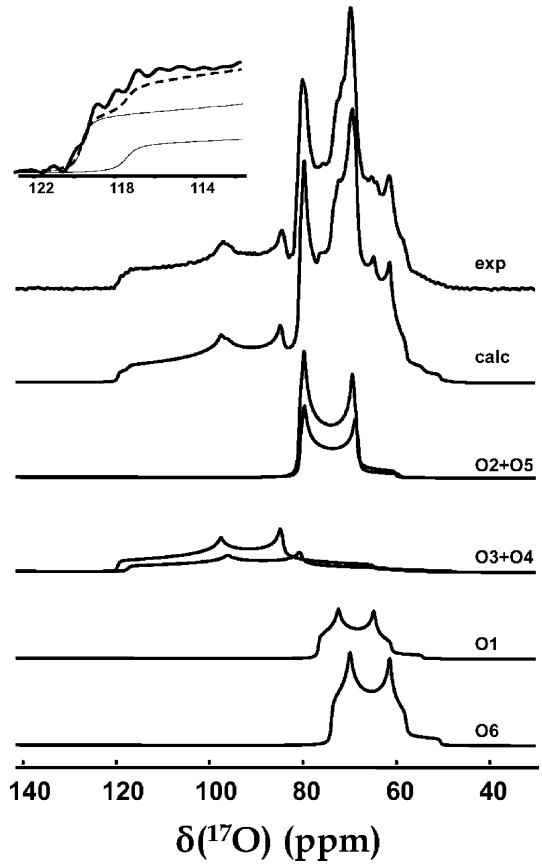

Figure 3. ^{17}O MAS NMR 1D spectrum of $Na_3P_3O_9$ is shown together with the individual lineshapes simulated using, as a starting point, NMR parameters from the DFT-GIPAW calculations for the optimized structure. (Top left inset) Expansion of the ^{17}O spectrum in the chemical shift region of bridging oxygens, with the calculated lineshapes for O3 and O4 sites (plain thin lines) and the resulting sum of the two contributions (dashed line).

nonbridging oxygens can be attributed to the direct observation of a J coupling between ^{17}O and ^{31}P nuclei. This attribution can be confirmed experimentally by identifying the small resonances on either sides of the Q^1 and Q^2 ^{31}P resonances as a contribution from the $^{17}O-^{31}P$ J coupling (cf. 1D MAS spectrum on the right of Figure 6). The simulation of the ^{17}O MAS spectrum (Figure 4) leads to a measured splitting between 120 and 130 Hz that is in the range of published values of nonbridging oxygen to phosphorus J coupling in solution[51] or in organic solids.[52]

The 2D 3QMAS spectrum (part b of Figure 5) clearly shows three resonances: one in the chemical shift range of bridging oxygens and two in the chemical shift range of nonbridging oxygens. Once again, we observe a discrepancy between the NMR results and the structural data as there are five crystallographically distinct oxygens. The assignment of the unique bridging oxygen is obvious, taking into account empirical considerations that have been mentioned above. The assignment of nonbridging ^{17}O sites can be achieved using the information provided by the correlation spectrum of Figure 6. It shows the $^{17}O\{^{31}P\}$MAS-J-HMQC spectrum

(49) Kristensen, J. H.; Farnan, I. *J. Chem. Phys.* **2001**, *114*, 9608.
(50) Schurko, R. W.; Wi, S.; Frydman, L. *J. Phys. Chem.* **2002**, *A106*, 51.
(51) Sammons, R. D.; Frey, P. A.; Bruzik, K.; Tsai, M.-D. *J. Am. Chem. Soc.* **1983**, *105*, 5455.
(52) Bryce, D. L.; Eichele, K.; Wasylishen, R. E. *Inorg. Chem.* **2003**, *42*, 5085.

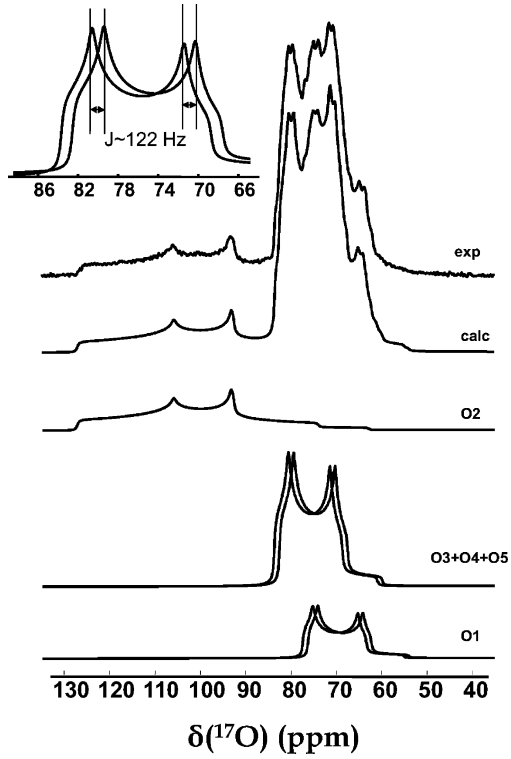

Figure 4. ^{17}O MAS NMR 1D spectrum of $Na_5P_3O_{10}$ (18.8 T) together with the individual lineshapes. The inset shows the measurement of ^{17}O−^{31}P *J* coupling constant on the O3, O4, and O5 sites simulation.

that correlates ^{17}O sites with chemically bonded ^{31}P. The ^{31}P spectrum of $Na_5P_3O_{10}$ (right side of the 2D spectrum) is composed mainly of two resonances at 1.3 and −7.5 ppm, which correspond to Q^1 and Q^2 phosphate groups, respectively. In Figure 6, only the chemical shift range of nonbridging oxygen is presented. Indeed, it was not possible to observe a correlation signal between bridging oxygens and phosphorus sites because of (i) the low intensity of this oxygen resonance and (ii) the possibly smaller *J*-coupling value for bridging oxygens compared to nonbridging oxygens. We observe two correlation signals for nonbridging oxygen sites. The top signal shows a correlation between one nonbridging ^{17}O site and the Q^2 phosphate group only. This signal can be assigned to oxygen site O1. The other correlation signal shows nonbridging oxygen sites, which are chemically bonded to Q^1 phosphorus sites only. They are assigned to O3, O4, and O5, respectively. This attribution is in agreement with the relative intensities obtained with the deconvolution of the 1D spectrum.

Table 3 summarizes the NMR parameters calculated with the GIPAW method for $Na_5P_3O_{10}$ using the same chemical shift reference than that used for $Na_3P_3O_9$. These results confirm the assignment deduced from the NMR experiments, especially for sites O1 and O2. The GIPAW results of end-chain sites O3, O4, and O5 require special attention. Indeed, one can clearly see that the computed NMR parameters for these three sites are slightly different and even in disagreement with previous experimental assignment. In part a of Figure 7, we plotted the experimental and calculated chemical shift values for nonbridging oxygens of $Na_3P_3O_9$ and $Na_5P_3O_{10}$. Part b of Figure 7 shows the same correlation throughout the entire chemical-shift range of both bridging and nonbridging oxygen sites. Except for tripolyphosphate sites O3, O4, and O5, the correlation is excellent with a regression coefficient close to 1. We propose that the apparent discrepancy between theoretical and experimental parameters is the result of a dynamical effect through the free rotation of the end-chain phosphate group around the P−O2 axis. An experimental confirmation of our interpretation would be obtained by recording high-resolved 1D spectrum at low temperature even if that would bring additional experimental difficulties to reach the same level of resolution. Such an experiment is beyond the scope of the present article.

5.3. Pyrophosphate $Na_4P_2O_7$. Figure 8 shows the ^{17}O MAS and 3QMAS spectra of $Na_4P_2O_7$. The MAS spectrum (a) reveals the presence of bridging oxygen O1 in the 80−120 ppm range. The most intense signal on the right corresponds to the crystallographically distinct nonbridging oxygen sites. There is no evidence of second-order quadrupolar lineshapes, which could help distinguish the six nonbridging oxygen sites. The region of nonbridging oxygen sites is exhibited on the 3QMAS spectrum (part b of Figure 8) (bridging oxygens are barely detected due to unfavorable ^{17}O enrichment). Unfortunately, the six nonbridging oxygen sites are not clearly separated on the 2D spectrum. Nevertheless, the apparent broad line shape cannot be attributed to a possible distribution of chemical shift because the crystallinity of the sample was checked through XRD and confirmed by the quality of the ^{31}P and ^{23}Na MAS spectra (not shown). In fact, the signal of each component adds up to form a large line shape that is spread over a chemical shift range of 10 ppm in the isotropic dimension, reinforcing the idea that the end-chain oxygens are crystallographically distinct but very close in terms of the NMR parameters.

The calculated NMR parameters for $Na_4P_2O_7$ are given in Table 3. Once again, bridging and nonbridging oxygen sites are clearly distinguished by their chemical shift and quadrupolar coupling constant. Our observation for the asymmetry parameter η_Q is somewhat different from the values published by Prochnow et al.[53] Indeed, they report a value of 0.6, close to what we measure for bridging oxygens but not for nonbridging oxygens. The values that we propose are more in line with those experimentally measured on the other sodium phosphates of the present work ($Na_3P_3O_9$, $Na_5P_3O_{10}$). A close look at the chemical shift values calculated for the six nonbridging oxygens confirms that the width of the nonbridging oxygen resonance, observed on the 3QMAS spectrum in Figure 8, is not due to distribution but to a juxtaposition of six resonances, spreading from 74.4 to 81.2 ppm (∼7 ppm). The lack of resolution along the isotropic dimension of the 3QMAS spectrum renders difficult the comparison of experimental and calculated data for $Na_4P_2O_7$. In particular, the quadrupolar parameters cannot be extracted from the individual slices. Nevertheless, the accuracy of the calculated data in the two previous cases, $Na_3P_3O_9$ and $Na_5P_3O_{10}$, increases the confidence in the results

(53) Prochnow, D.; Grimmer, A.-R.; Freude, D. *Solid State Nucl. Magn. Reson.* **2006**, *30*, 69.

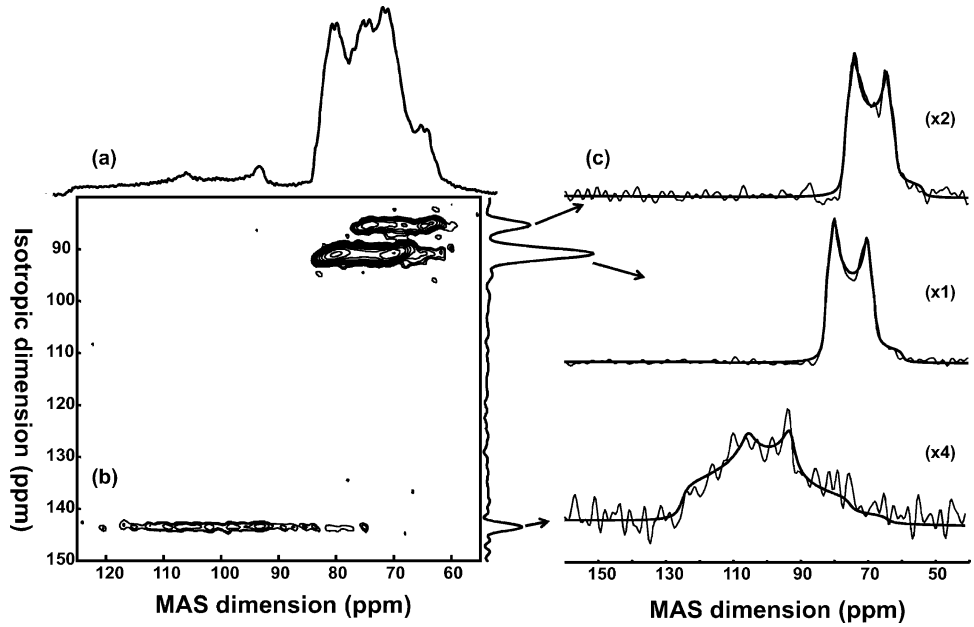

Figure 5. ^{17}O NMR of $Na_5P_3O_{10}$ (18.8 T). (a) The ^{17}O MAS spectrum required 64 scans with a recycling time of 60 s; (b) 3QMAS spectrum, a total of 12 scans was accumulated with a recycling delay of 20 s and 140 transients in the t_1 domain for an experimental time of ~10 h; (c) ^{17}O isotropic spectrum together with the extracted individual slices and corresponding fit simulations.

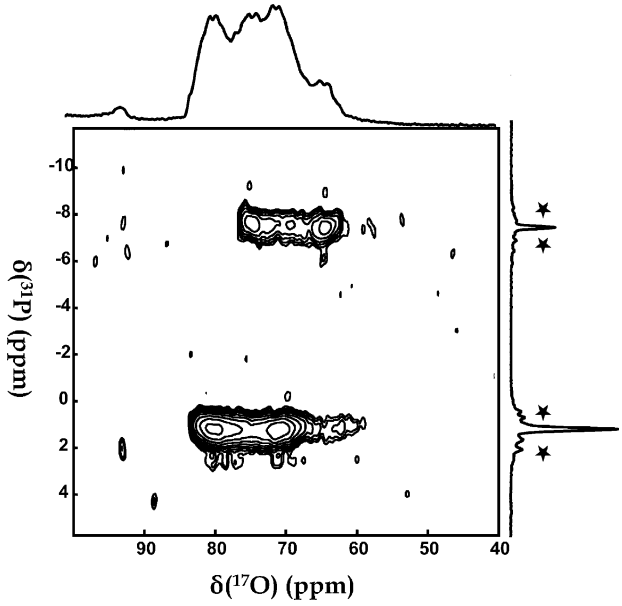

Figure 6. $^{17}O\{^{31}P\}$ MAS-J-HMQC of $Na_5P_3O_{10}$. ^{17}O (top) and ^{31}P (right) 1D MAS spectra are also presented for comparison with 2D spectrum. The 2D spectrum required a total of 16 scans with a recycling delay of 60 s and 50 t_1 increments (experimental time of 13 h). Note that the signal truncation in the t_1 dimension leads to a strong broadening of the ^{31}P line shape, to be compared with the high resolution of the 1D MAS spectrum (right). The stars in the ^{31}P MAS spectrum denote the multiplet resulting from the $^{17}O\{^{31}P\}$ J coupling.

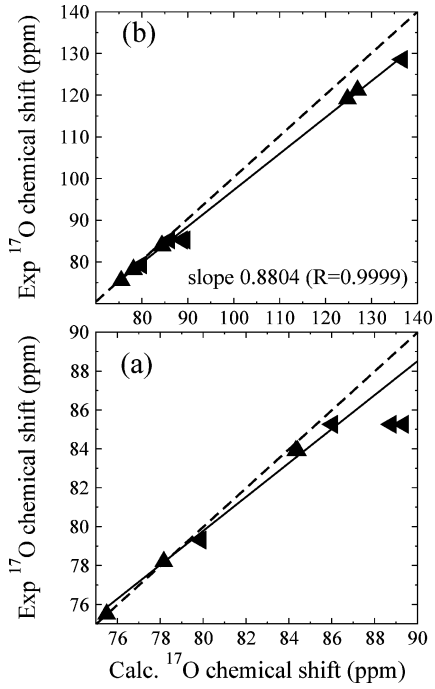

Figure 7. Correlation of experimental and calculated chemical shifts (δ_{iso}) for (a) nonbridging oxygens and (b) all sites. For the left solid triangle, the tripolyphosphate ($Na_5P_3O_{10}$) and (▲) the trimetaphosphate ($Na_3P_3O_9$), using the DFT optimized structures. The exact correlation between experiments and calculations is represented with a dashed line. The slope of linear regression is given with the correspondely regression coefficients (R).

obtained for $Na_4P_2O_7$. It is observed that C_Q and η_Q are also distributed over about 0.2 MHz and 0.1, respectively.

6. Discussion

We have seen in the previous sections that there is sometimes a discrepancy between experimental NMR results and structural data for the different model systems (particularly $Na_3P_3O_9$ and $Na_5P_3O_{10}$). Our work demonstrates that the DFT results provide the way to link the ^{17}O local environment to the NMR response.

Figure 9 integrates all the possible correlations between experimental and calculated values for the different NMR parameters (δ_{cs}, C_Q, η_Q) and for the two structures of $Na_3P_3O_9$ and $Na_5P_3O_{10}$ used in this work, that is, published structures and DFT optimized structures. The data obtained for $Na_4P_2O_7$ are excluded as they lack experimental resolution. The end-chain oxygen sites in $Na_5P_3O_{10}$ are omitted due to the dynamical effect, which seems to affect these sites. For

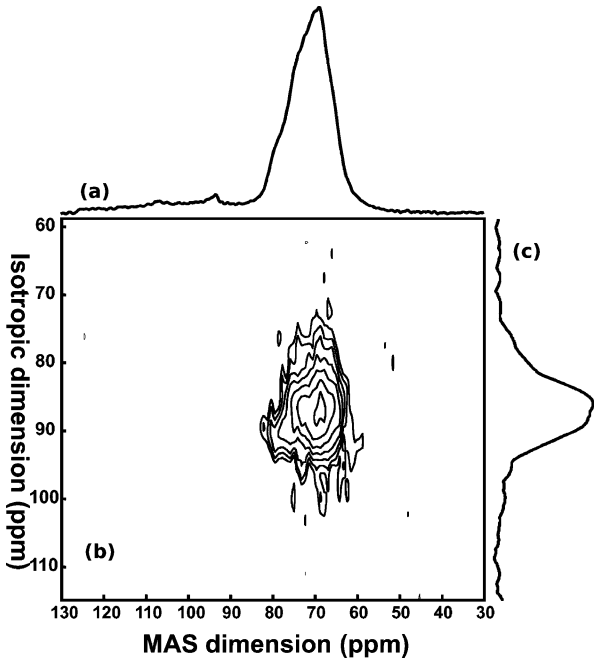

Figure 8. ^{17}O NMR of $Na_4P_2O_7$ (18.8 T). (a) The ^{17}O MAS spectrum required 4096 scans with a recycling time of 5 s. (b) 2D 3QMAS spectrum. A total of 432 scans was accumulated with a recycling delay of 5 s and 64 increments in the t_1 domain for a total experimental time of 38 h. (c) The isotropic ^{17}O 3QMAS spectrum.

clarity, we represented the chemical shift and the C_Q values to the limited range of nonbridging oxygens, even though the linear regression of the correlation is provided for all sites.

For the isotropic chemical shift, the slope of the correlation is smaller than one for the optimized structures (right) and close to one for the published structures (left). However, one can clearly observe that the optimized structure reveals a better correlation between experimental and theoretical results, which is fundamental for the assignment. The regression coefficient is therefore an important and accurate parameter that helps to select the best structure for an optimal fit of the experimental NMR results. The regression coefficients are also given in Figure 9 for the quadrupolar parameters (b, e) C_Q and (c, f) η_Q. For both parameters, the DFT-optimized structures provide systematically a better correlation than the original published structures.

The present results clearly demonstrate that the long-distance order governs the oxygen chemical shift in phosphates. Indeed, only a periodic approach reproduced the correct spectra. A cluster-based calculation, considering either the anion or the first coordination sphere within the same systems (not shown), gives incoherent results compared to the experimental ones. A close look at the chemical shift values for nonbridging oxygens in $Na_3P_3O_9$ can further demonstrate which structural feature influences the chemical shift. As explained in the results section, the oxygen sites O2 and O5 are completely equivalent in terms of NMR parameters, whereas they have different first coordination spheres (Figure 10). Focusing on the first coordination sphere only, it even appears that site O2 looks similar to O6, and O5 looks similar to O1. Our experimental and calculated results of the chemical shift for nonbridging oxygens

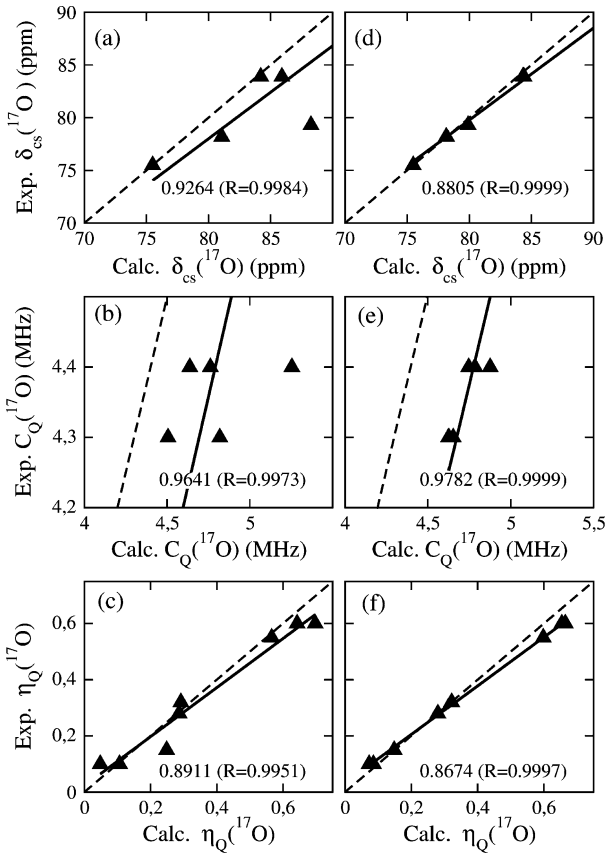

Figure 9. Comparaison of experimental and calculated NMR parameters (δ_{iso}, C_Q, η_Q) for (a, b, c) the published structures and (d, e, f) the DFT optimized structure of trimetaphosphate ($Na_3P_3O_9$) and tripolyphosphate (for $Na_5P_3O_{10}$, sites O1, O2, only). For δ_{iso} and C_Q parameters, the graphs are restricted to the range of the nonbridging oxygens. The exact correlation between experimental and calculated values is represented by a dashed line. The slope of the linear regression is given with corresponding regression coefficients (R).

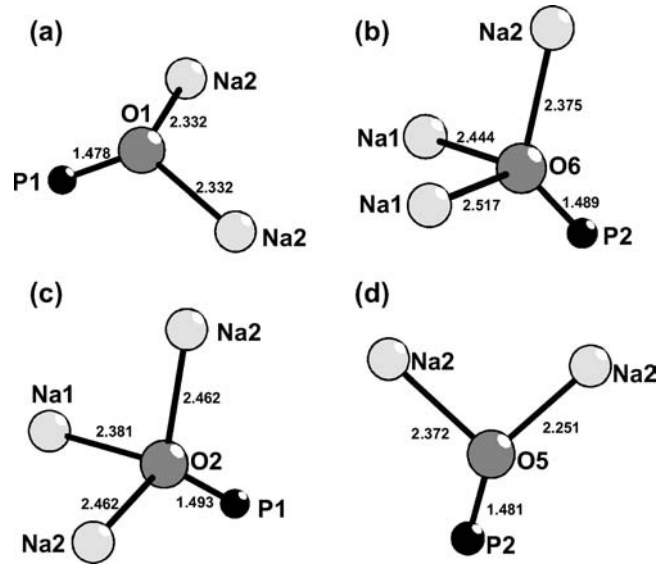

Figure 10. First sphere of coordination of different nonbridging oxygens in trimetaphosphate ($Na_3P_3O_9$) with the corresponding distances between sites obtained after the optimized DFT structure. (a) O1, trigonal site; (b) O6, tetrahedral site; (c) O2, tetrahedral site; and (d) O5, trigonal-planar site.

therefore clearly show that the long-range structural organization prevails. Following this, we conclude that the ^{17}O

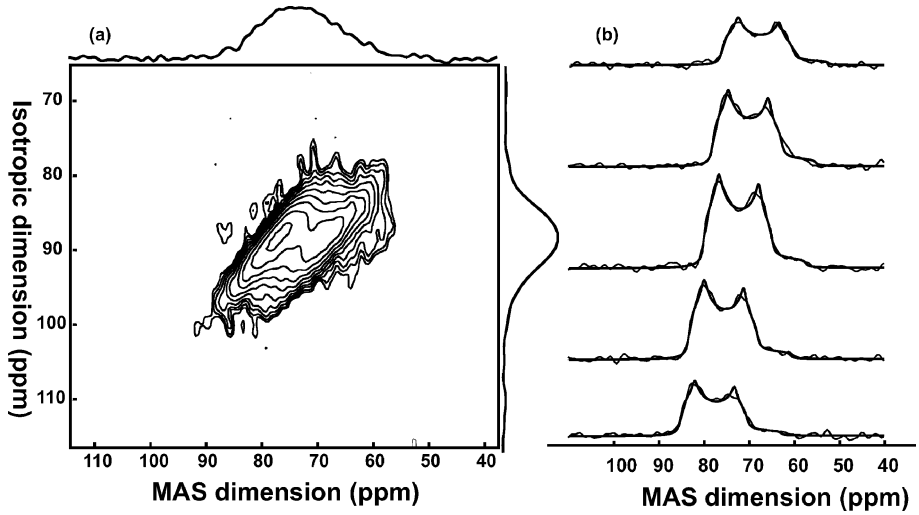

Figure 11. ^{17}O MQMAS NMR of sodium metaphosphate glass (18.8 T). (a) ^{17}O 2D 3QMAS spectrum, a total of 876 scans was accumulated with a recycling delay of 0.8 s and 40 t_1 increments for an experimental time of about 8 h. (b) Five slices are extracted from the 2D spectrum and shown with their respective best fit simulation.

chemical shift in phosphates cannot be used to differentiate local structure and geometry within a type of coordination. This may be due to a large sensitivity of the local electronic structure of nonbridging oxygen with respect to the large-range electrostatic potential.

We also demonstrate that in contrast with δ_{cs}, the C_Q and η_Q parameters in sodium phosphates are clearly determined by the nature of the local environment. Indeed, we verified that for bridging oxygens in $Na_3P_3O_9$, it is possible to match the C_Q and η_Q values with the empirical angular correlation that was constructed from a cluster-based calculation performed on a simple $H_4P_2O_7$.[20]

The quadrupolar parameters C_Q and η_Q can further be interpreted in terms of local coordination and geometry. Indeed, within the group of nonbridging oxygens in $Na_3P_3O_9$, one can observe two domains that separate sites O2 (4.74 MHz) and O6 (4.78 MHz) on the one hand and sites O1 (4.65 MHz) and O5 (4.62 MHz) on the other hand. These groups can be chemically distinguished by their first coordination sphere as shown in Figure 10. The C_Q parameter can therefore be interpreted as a semilocal probe, sensitive to the oxygen coordination. In the case of the η_Q parameter, the nature of the first coordination sphere does not seem to matter. Indeed, nonbridging oxygen sites are grouped into two groups {O2,O5} and {O1,O6}, which are related to their axial or equatorial positions on a cyclohexane-like molecule rather than the nature and number of sodium sites. The conclusion is thus that the ^{17}O η_Q parameter in phosphates is a local probe, which is sensitive to the geometry of the P$-^{17}$O bond in the phosphate group.

It is important to note that the structure optimization is much more critical for C_Q than for η_Q because C_Q values for nonbridging oxygens are within a small range of 0.2 MHz. This result points out the fact that nonbridging oxygen sites in sodium phosphates can not be characterized by their experimental C_Q values solely. On the other hand, the η_Q values can because they spread over a broad range. The bridging oxygen values clearly appear around 0.6. For nonbridging oxygens, the η_Q values are found to be within a broad range of about 0.3 (from 0.1 to 0.4). In this case, it seems possible to further correlate a specific nonbridging oxygen environment with the corresponding η_Q parameter. Nevertheless, such correlation would require (i) a better experimental determination of the η_Q parameter and (ii) a more complete database of sodium phosphate reference compounds.

Table 4. NMR Parameters Extracted by Fitting Five Individual Anisotropic Slices of 3Q Filtered Spectrum for $NaPO_3$ Glass[a]

C_Q (MHz)	η_Q	δ_{cs} (ppm)
4.5	0.25	78.27
4.4	0.24	80.07
4.4	0.24	82.04
4.4	0.24	85.37
4.3	0.23	87.29

[a] The sites are organized from low to high chemical shifts.

These conclusions enable the interpretation of ^{17}O NMR spectrum of a sodium metaphosphate glass ($NaPO_3$) by NMR. Part a of Figure 11 represents the ^{17}O 3QMAS spectrum of $NaPO_3$ glass restricted to the chemical shift range of nonbridging oxygens. Part b of Figure 11 represents five arbitrary anisotropic slices and their respective simulation. Here, we clearly observe a distribution in chemical shift without line shape modification. This is confirmed by the result of the best fit simulations summarized in Table 4. It can be observed that only the δ_{cs} parameter is subjected to a large variation within this compound and the other parameters (C_Q, η_Q) vary by only 0.1 and 0.02 MHz, respectively. Note that the typical second-order quadrupolar feature is still present with sharp discontinuities, close to those that are observed on MAS spectra of crystalline phosphates. Therefore, the glass structure is clearly amorphous in a long range, as deduced from the large variation of δ_{cs}, the only parameter sensitive to a long-range disorder. On the other hand, the local environment in the glass does not seem to change much, as shown by the quadrupolar parameters − used as a local probe − that are quasi-constant. The structure description provided here through the inter-

pretation of the NMR parameters is consistent with common description of amorphous systems.

7. Conclusion

The ^{17}O MAS NMR spectra of a series of three sodium phosphate compounds was interpreted through the combination of high-resolution NMR experiments and periodical DFT calculations. The correlation of experimental and theoretical parameters depends on the quality of the initial structure. The DFT-optimized structures always leads to a better match. Two of the sodium phosphate systems presented here were used provide a set of data that help in the interpretation of the NMR parameters in terms of local, η_Q, semilocal, C_Q, and long-range, δ_{cs}, geometry, and coordination. These observations were finally applied to the structural description of a binary glass, $NaPO_3$. The strong distribution of chemical shift reveals the long-range disorder in the glass, whereas the absence of variation of C_Q and η_Q parameters demonstrates the persistence of an order within the oxygen first-coordination sphere.

Acknowledgment. The USTL Centre de Ressources Informatiques and IDRIS are acknowledged for the allocating of CPU time. F.V. is supported by the Ministère de l′Éducation Nationale de l'Enseignement Supérieure et de la Recherche. The FEDER, Région Nord Pas-de-Calais, Ministre de l′Éducation Nationale de l'Enseignement Supérieure et de la Recherche, CNRS, and USTL are acknowledged for financial support.

Supporting Information Available: This material is available free of charge via the Internet at http://pubs.acs.org.

IC800637P